Metasurface holograms reaching 80% efficiency

Zheng, Guoxing; Zhang, Shuang; Li, Guixin; Kenney, Mitchell; Mühlenbernd, Holger; Zentgraf, Thomas

DOI:
10.1038/nnano.2015.2

Metasurface holograms reaching 80% efficiency

Guoxing Zheng[1, 2*], Holger Mühlenbernd[3*], Mitchell Kenney[1*], Guixin Li[4†], Thomas Zentgraf[3‡] and Shuang Zhang[1§]

1. *School of Physics & Astronomy, University of Birmingham, Birmingham, B15 2TT, UK*
2. *School of Electronic Information, Wuhan University, Wuhan, 430072, China*
3. *Department of Physics, University of Paderborn, Warburger Straße 100, D-33098 Paderborn, Germany*
4. *Department of Physics, Hong Kong Baptist University, Hong Kong, China*

Surfaces covered by ultrathin plasmonic structures, so called metasurfaces[1-4], have been recently shown to be capable of completely controlling the phase of light, representing a new paradigm for the design of innovative optical elements, such as ultrathin flat lenses[5-7], directional coupler for surface plasmon polaritons[4, 8-10], and wave plates for generating vortex beams[1, 11]. Among various types of metasurfaces, geometric metasurfaces (GEMS) that consist of an array of plasmonic nanorods with spatially varying orientations, have shown superior phase control due to the geometric nature of the phase[12, 13]. Metasurfaces have been recently utilized to realize computer generated holograms (CGHs)[14-19]. However, hologram efficiencies remain too low at visible wavelengths for practical purposes. Here we report the design and realization of GEMS holograms reaching diffraction efficiencies of 80% at 825 nm and a broad bandwidth between 630 nm and 1050 nm. Our design comprises a 16-level phase CGH design, which combines the concept of GEMS for the superior control of the phase profile and the concept of reflectarrays for achieving high polarization conversion efficiency. Specifically, our design features the incorporation of a ground metal plane to GEMS for dramatically enhancing the conversion efficiency between the two circular polarization states, leading to very high diffraction efficiency without complicating the fabrication process. Because of these advantages, our strategy could be viable for various holographic applications.

In traditional phase-only computer generated hologram designs, the phase profile is controlled by etching different depths into a transparent substrate. Due to the ease of fabrication, two level binary CGHs have been widely employed. Such CGHs have a theoretical diffraction efficiency of only 40.5% and the issue of twin-image generation cannot be avoided. Multi-level phase CGHs can alleviate the problem of low efficiency and twin-image generation; however, fabricating such CGHs requires expensive and complicated grayscale lithography, variable-dose, or multi-step lithography[20]. Furthermore, the unavoidable etching error, resolution error and alignment error can dramatically degrade the performance of CGHs, such as low signal-to-noise ratio, poor

* These authors contributed equally to this work.
† gxli@hkbu.edu.hk
‡ thomas.zentgraf@uni-paderborn.de
§ s.zhang@bham.ac.uk

uniformity and strong zero-order intensity. To obtain a higher efficiency and less manufacturing complexity, an effective medium approach has been proposed[20], where two-level depth subwavelength structures with variable cell dimension can function as an effective medium with geometry controlled effective refractive index, and consequently act as a multi-level CGH. However, such a design involves extreme small feature sizes with high aspect ratios, limiting the observed efficiency of a three level CGH to less than 30%, which is significantly lower than the theoretical value of 48%.

GEMS provide an alternative approach towards high efficiency holograms without complicated fabrication procedures. The operation of GEMS relies on the inversion of the absolute rotation direction of the electric field of the radiation (in transmission or reflection) compared to that of the incident circularly polarized one[21, 22]. This is equivalent to flipping the circular polarization in transmission or maintaining the same circular polarization in reflection. A geometric phase, or Pancharatnam-Berry phase, is acquired through the inversion of electric field rotation, leading to an antenna-orientation controlled phase which does not depend on the specific antenna design or wavelength, thus making its performance broadband, and highly robust against fabrication latitude and variation of material properties. However, GEMS operating at visible and near infrared wavelengths have been limited so far by the low efficiency in conversion between the two circular polarization states.

In order to increase the efficiency of GEMS, a multilayer design is employed for achieving high polarization conversion[23-26]. The reflective metasurface hologram consists of three layers: a ground metal plane, a dielectric spacer layer and a top layer of antennas (Figure 1). It is well known that a half wave plate can fully convert a circular polarized beam to the oppositely polarized one in transmission due to a phase delay of π between the fast and slow axis. Hence, for achieving high conversion between the two circular polarization states, it is desired that the phase difference between the reflection with polarization along the long axis (r_l) and short axis (r_s) of the nanorod antenna equals π. The simulated results in Figure 1d-e show that, with an optimized configuration, the phase difference between the reflection coefficients r_l and r_s approaches π within a wide wavelength range of 600-1000 nm. At the same time, the configuration maintains very large reflection amplitudes over 0.8 for both linear polarizations. Therefore, regardless the orientation of the antennas, it is expected that the circularly polarized incident light almost completely flips the absolute rotation direction of the electric field upon reflection, thus preserving its circular polarization state considering that the wave vector is reversed as well. This forms the basis of the high efficiency geometric metasurface. A detailed discussion and a simplified model for explaining the high efficiency and broadband responses of the nanorod metasurface can be found in the SI (Supplementary Fig. 1-7).

The high efficiency of maintaining the same circular polarization state upon reflection is verified by numerical simulations for a uniform metasurface with all nanorod antennas aligned along the same direction, as shown in Figure 1f. The reflected wave in general consists of both circular polarization states: one is the same handedness as the incident circularly polarized light but with an additional phase delay 2ϕ, where ϕ is the orientation angle of the nanorod antenna, and the other one is the opposite handedness without the additional phase delay. For the specific

geometry configuration shown in Figure 1a upon normal light incidence, the numerical simulation shows that the reflectivity of light with the same circular polarization state is over 80% in a broad wavelength range between 550 nm and 1000 nm, covering nearly a full optical octave. This efficiency is surprisingly high considering the ohmic loss of metal at the visible and near infrared frequencies. Interestingly, the the ohmic loss in our configuration is very close to that of light transmitting through a single metasurface layer (without the ground metal plane) around the resonance wavelength (800 - 850 nm) of the antenna (Supplementary Fig. 8). On the other hand, the efficiency of the unwanted opposite polarization is extremely low, less than 3%, over a broad wavelength range.

To confirm the high efficiency of our numerical simulations we designed a geometric metasurface based CGH as shown in Figure 2. The CGH was designed for circularly polarized light at normal incidence. We used a design so that the holographic image appears off-axis to avoid the overlapping between the holographic image and the zero-order spot. The CGH is designed to create a wide image angle of 60°×30°. In our structure we used a 2×2 periodic array of the hologram pattern (Figure 2d), more details of the advantages of the 2x2 periodic arrangement over single hologram is given in the SI (Supplementary Fig. 9). To create an holographic image with a pixel array of $m \times n$ within the angular range of $\alpha_x \times \alpha_y$ in the far field, the period of the CGH at x and y direction can be calculated by $d_x = m\lambda/[2\tan(\alpha_x/2)]$ and $d_y = n\lambda/[2\tan(\alpha_y/2)]$, respectively. The number of pixels of the CGH is determined by $M = d_x/\Delta p$ and $N = d_y/\Delta p$, where Δp is the pixel size of the CGH in both x and y directions.

With the above structural parameters, a phase-only CGH with pixel size of 300 nm × 300 nm and periods of 333.3 μm × 333.3 μm was designed by the classical Gerchberg–Saxton algorithm[27]. Note that the size of the pixel along each direction is less than half of the wavelength, ensuring that the hologram pattern is sampled at least at twice the maximum spatial frequency in either direction, which satisfies the Shannon-Nyquist sampling theorem. The obtained phase distribution for the hologram is shown in Figure 2c. In the CGH design, we take the conversion efficiency, signal-to-noise ratio and uniformity as merit functions for optimization. Since the phase delay is determined solely by the orientation of the nanorod antennas, 16 phase levels (Figure 1c) are used to obtain a high performance of the CGH. Simulation shows that in our optimized design with an ideal hologram neglecting optical losses, the window efficiency, which is defined as the ratio between the optical power projected into the image region and the input power, reaches 94%.

The metasurface CGH is fabricated on top of a Silicon substrate following the design described above (Figure 3a). The simulated and measured holographic images, including both the zoomed-in views of the face and the letter ‘M’, show good agreement with each other. This demonstrates the extremely high fidelity of the metasurface hologram. To determine the conversion efficiency, the linear polarization state of light from a super continuum light source (Fianium supercontinuum) is converted to circular polarization by using a linear polarizer and a quarter waveplate. The reflected holographic image is collected by two condenser lenses with high numerical aperture and the hologram image was measured in the range from 600 nm to 1100 nm in steps of 25 nm. The optical efficiency (holographic window efficiency) is finally

determined by subtracting the 0^{th}-order beam signal from the image intensity (Figure 3b). We find a relatively broad spectral range from 630 nm to 1050 nm with high window efficiency larger than 50% that reaches its maximum of 80% at a wavelength of 825 nm. At the same time the unwanted 0^{th}-order efficiency is only around 2.4%. More importantly, we do not observe the twin image effect that traditional binary holograms usually suffer from.

Theoretically the metasurface hologram has an even broader spectral response (Figure 1f) when compared to the measured efficiency. The lower bandwidth likely arises from the fact that the calculated conversion efficiency is obtained on a metasurface under normal incidence. Whereas in the experiment the holographic image from the metasurface hologram is projected into a broad angular range. We expected that this broad angle scattering induces the narrower bandwidth and lower peak reflection than the calculated results shown in Figure 1f. A detailed discussion of the diffraction efficiency of the metasurface consisting of nanoantennas with nonuniform orientations is given in the SI (Supplementary Fig. 10, 11). In addition, a weak near-field coupling effect among neighboring nanorod antennas introduces a small phase deviation compared to the design (Supplementary Fig. 12).

In summary, we have presented a reflective phase-only hologram based on geometric metasurfaces that shows a diffraction efficiency as high as 80%, an extremely low 0^{th}-order efficiency and a broadband spectral response in the visible/near-IR range. Our metasurface has an ultrathin and uniform thickness of 30 nm and is compatible with the scalar diffraction theory even for subwavelength pixel sizes[28], thus simplifying the design of holograms. Given its simple and robust phase control, its good tolerance to wavelength variations and fabrication errors, our geometric phase based CGH design could overcome the current limitations of traditional depth-controlled CGH and find application in fields such as laser holographic keyboard, random spots generator for body motion, optical anti-counterfeiting, and laser beam shaping. Moreover, our approach can be readily extended from phase-only to amplitude-controlled holograms simply by changing the size of the nanorods. Since we exploit a phase effect due to polarization state change, the only restriction of our technique is the fact that the polarization state of the light cannot be controlled, that is, the incident light has to be circularly polarized. Finally, we would like to note that such nanorod metasurfaces could be fabricated on a large scale and much lower costs by nano-imprinting, thus making them promising candidates for large-scale holographic technology.

Methods:

1. Simulation of the conversion efficiency. The nanorod cell was designed and simulated by CST microwave studio software. In the simulation, a linearly polarized plane wave is normally incident onto a single nanorod with periodic boundary conditions. The spectra of reflection coefficients r_{xx}, r_{xy}, r_{yy}, r_{yx} are obtained from the simulation. From the reflection of linear polarized light we can retrieve the reflection coefficients for circularly polarized light as $r_{rr}= [r_{xx}+r_{yy}- (r_{xy}-r_{yx})\cdot i]/2$ and $r_{lr}=[r_{xx}-r_{yy}-(r_{yx}+r_{xy})\cdot i]/2$. The performance of the nanorods is optimized by sweeping the geometric parameters of the nanorod including the cell size, spacer and gold thickness.

2. Design of metasurface hologram. In the design, a complex digital image containing Einstein's

portrait (copyright license from Free Stock Photos http://publicdomainpictures.net/view-image.php?image=8612) with pixel number of 550×300 and 256 greyscale levels was chosen as holographic target image (Figure 2b). Because of the large angular range, the Rayleigh-Sommerfeld diffraction method is used to simulate the holographic image[29]. The hologram is pre-compensated to avoid the pattern distortion. To avoid the formation of laser speckles in the holographic image, the concept of Dammann gratings[30] is utilized for the hologram design.

3. Fabrication and experimental setup. The samples are fabricated on a gold and MgF_2-coated Silicon substrate with standard electron-beam lithography, subsequent deposition of 30 nm gold and lift-off processes. For the imaging experiment, we used a red laser (He-Ne laser, wavelength of 632.8 nm) and a near infrared diode laser (780 nm). The circularly polarized laser source is incident onto the metasurface hologram, and the reflected holographic image is projected onto a white screen 300 mm away from the surface of the hologram. We captured the red and near infrared holographic image by using commercial digital cameras (Nikon D3200 and ELOP-Contour CMOS IR Digital Camera). For optical efficiency measurement, one can find the details of experimental setup, efficiency calculation and incident angle scanning in the SI (Supplementary Fig. 13-15).

References:

1. Yu, N. et al. Light propagation with phase discontinuities: generalized laws of reflection and refraction. *Science* 334, 333-337 (2011).

2. Ni, X., Emani, N. K., Kildishev, A. V., Boltasseva, A. & Shalaev, V. M. Broadband light bending with plasmonic nano antennas. *Science* 335, 427 (2012).

3. Sun, S. et al. Gradient-index meta-surfaces as a bridge linking propagating waves and surface waves. *Nature Mater*. 11, 426-431 (2012).

4. Yin, X., Ye, Z., Rho, J., Wang, Y. & Zhang, X. Photonic spin hall effect at metasurfaces. *Science* 339, 1405-1407 (2013).

5. Aieta, F. et al. Aberration-free ultrathin flat lenses and axicons at telecom wavelengths based on plasmonic metasurfaces. *Nano Lett*. 12, 4932-4936 (2012).

6. Chen, X. et al. Dual-polarity plasmonic metalens for visible light. *Nature Comm*. 3, 1198 (2012).

7. Ni, X., Ishii, S., Kildishev, A. V. & Shalaev, V. M. Ultra-thin, planar, Babinet-inverted plasmonic metalenses. *Light Sci. & Appl*. 2, e72 (2013).

8. Lin, J. et al. Polarization-controlled tunable directional coupling of surface plasmon polaritons. *Science* 340, 331-334 (2013).

9. Huang, L. et al. Helicity dependent directional surface plasmon polariton excitation using a metasurface with interfacial phase discontinuity. *Light Sci. & Appl*. 2, e70 (2013).

10. Shitrit, N. et al. Spin-optical metamaterial route to spin-controlled photonics. *Science* 340, 724-726 (2013).

11. Li. G. et al, Spin Enabled Plasmonic Metasurfaces for Manipulating Orbital Angular Momentum of Light, Nano Letters, 11, 4148 (2013)

12. Dahan, N., Gorodetski, Y., Frischwasser, K., Kleiner, V., and Hasman, E., Geometric Doppler Effect: Spin-Split Dispersion of Thermal Radiation, Phys. Rev. Lett., 105, 136402 (2010)

13. Huang, L. et al. Dispersionless phase discontinuities for controlling light Propagation. *Nano Lett*. 12, 5750-5755 (2012).

14. Larouche, S., Tsai, Y. J., Tyler, T., Jokerst, N. M., & Smith, D. R. Infrared metamaterial phase holograms. *Nature Mater.* 11(5), 450-454 (2012).

15. Chen, W. T. et al. High-efficiency broadband meta-hologram with polarization-controlled dual images. *Nano Lett.* 14(1), 225-230 (2013).

16. Yifat, Y., Eitan, M., Iluz, Z., Hanein, Y., Boag, A., & Scheuer, J. Highly Efficient and Broadband Wide-Angle Holography Using Patch-Dipole Nanoantenna Reflectarrays. *Nano Lett.* 14(5), 2485-2490 (2014).

17. Huang, L.et al. Three-dimensional optical holography using a plasmonic metasurface. *Nature Commun.* 4 (2013).

18. Ni, X., Kildishev, A. V., & Shalaev, V. M. Metasurface holograms for visible light. *Nature Commun*. 4 (2013).

19. Lin, J., Genevet, P., Kats, M.A., Antoniou, N., & Capasso, F. Nanostructured holograms for broadband manipulation of vector beams. *Nano Lett.* 13(9), 4269-4274 (2013).

20. Freese, W., Kämpfe, T., Kley, E. B., & Tünnermann, A. Design of binary subwavelength multiphase level computer generated holograms. *Optics Lett.* 35(5), 676-678(2010).

21. F. Gori, Measuring Stokes parameters by means of a polarization grating, Opt. Lett. 24, 584 (1999).

22. Bomzon, Z., Biener, G., Kleiner, V., and Hasman, E., Space-variant Pancharatnam–Berry phase

optical elements with computer-generated subwavelength gratings, Opt. Lett. 27, 1141 (2002)
23. Hao, J. et al. Manipulating Electromagnetic Wave Polarizations by Anisotropic Metamaterials, *Phys. Rev. Lett.* 99, 063908 (2007).
24. Pors, A., Nielsen, M. G., & Bozhevolnyi, S. I. Broadband plasmonic half-wave plates in reflection. *Optics Lett.* 38(4), 513-515 (2013).
25. Grady, N. K. et al. Terahertz Metamaterials for Linear Polarization Conversion and Anomalous Refraction, *Science* 340, 1304 (2013).
26. Jiang, S. C., Xiong, X., Hu, Y. S., Hu, Y. H., Ma, G. B., Peng, R. W., Sun, C., and Wang, M., Controlling the Polarization State of Light with a Dispersion-Free Metastructure, Phys. Rev. X 4, 021026 (2014).
27. Gerchberg, R. W. & Saxton, W. O. A practical algorithm for the determination of phase from image and diffraction plane pictures. *Optik* 35, 237 (1972).
28. Hasman, E., Davidson, N., & Friesem, A. A. Efficient multilevel phase holograms for CO_2 lasers, *Opt. Lett.* 16, 423 (1991).
29. Shen, F., & Wang, A. Fast-Fourier-transform based numerical integration method for the Rayleigh-Sommerfeld diffraction formula. *Appl. Opt*. 45(6), 1102-1110 (2006).
30. Dammann, H., & Görtler, K. High-efficiency in-line multiple imaging by means of multiple phase holograms. *Opt. Comm.* 3(5), 312-315, (1971).

Acknowledgement
The research is partly supported by EPSRC (EP/J018473/1). We thank Lingxiao Zhu and Wei He for fruitful discussions. H. M. and T. Z. acknowledge the financial support by the DFG Research Training Group GRK1464. S. Z. and T. Z. acknowledge the European Commission under the Marie Curie Career Integration Program. S. Z. acknowledges the financial support from NSFC (Grant # 61328503).

Author contributions
G. Z., T. Z., G. L. and S. Z. conceived and designed the experiments: M. G. and G. Z. performed the design and simulation on the metasurfaces: H. M. fabricated the samples: G. Z. and G. L. performed the measurements: G. Z., G. L., T. Z. and S. Z. analyzed the data: G. Z., S. Z. and T. Z. co-wrote the paper. All authors discussed the results and commented on the manuscript.

Additional information
Supplementary information accompanies this paper at www.nature.com/naturenanotechnology. Reprints and permission information is available online at http://npg.nature.com/reprintsandpermissions/. Correspondence and requests for materials should be addressed to T. Z. and S. Z.

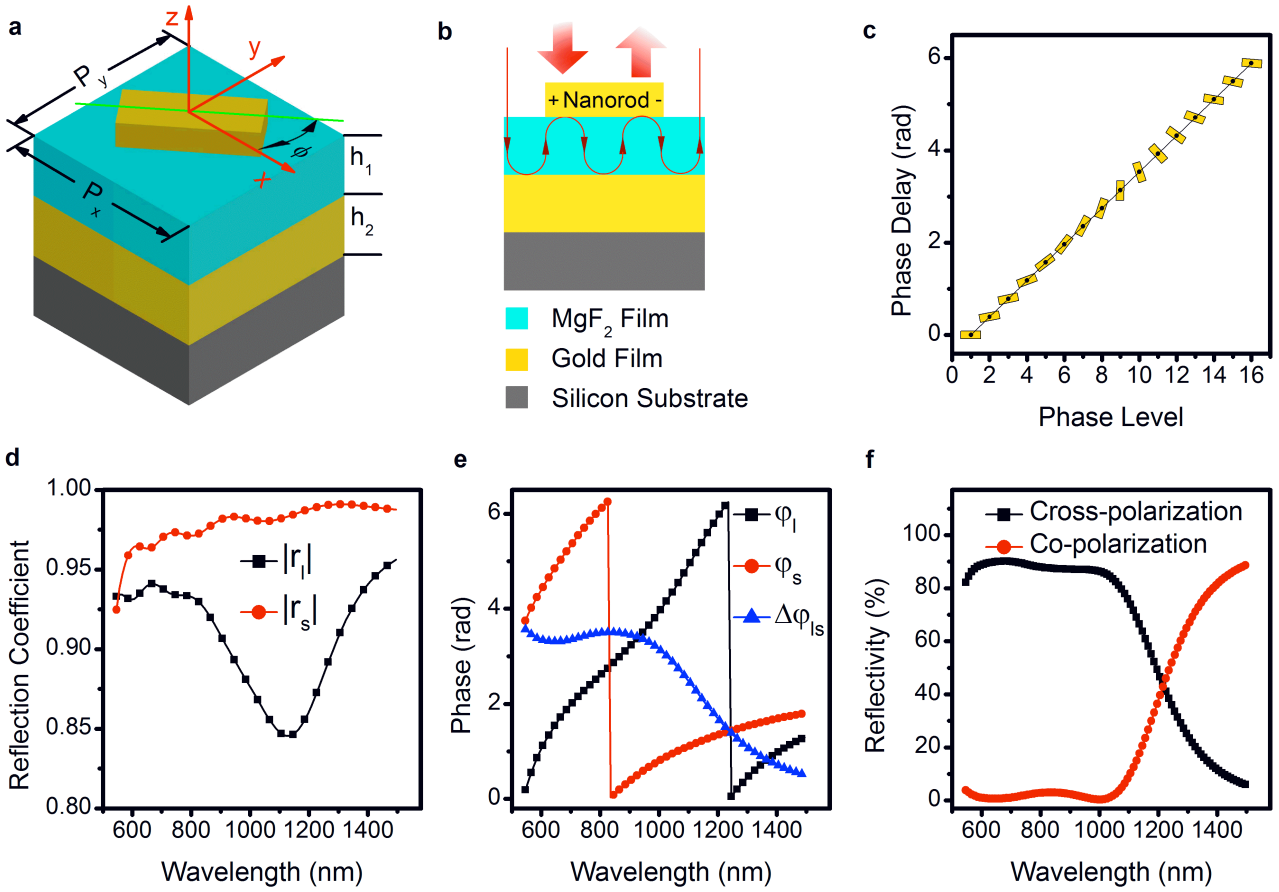

Figure 1 | Illustration of the unit-cell structure and its polarization conversion efficiency by numerical simulations. a, One pixel cell structure of the nanorod based hologram. The nanorod can rotate in the x-y plane with an orientation angle ϕ to create different phase delay. The pixels are arranged with periods P_x=300 nm and P_y=300 nm. The nanorods have a length of L=200 nm, a width of W=80 nm and a height of H=30 nm. The MgF_2 and gold film have thicknesses of h_1=90 nm and h_2=130 nm, respectively. **b**, Cross section of the pixel cell. The MgF_2 film acts as a Fabry-Pérot cavity, which can let the returned beam keep exciting the nanorod and generate the output beam with phase-delay. The gold film acts as the mirror to reflect the incident light. **c**, Phase delay for the different phase levels. On each knot, the orientation of nanorod has been annotated. **d and e**, Simulated amplitude $|r_l|$, $|r_s|$, phase φ_l, φ_s and phase difference $\Delta\varphi_{ls}$ of the reflection coefficients r_l and r_s, where l and s denote the long and short axis directions of the nanorods, respectively. **f**, Simulated cross-polarization and co-polarization reflectivity upon normal light incidence.

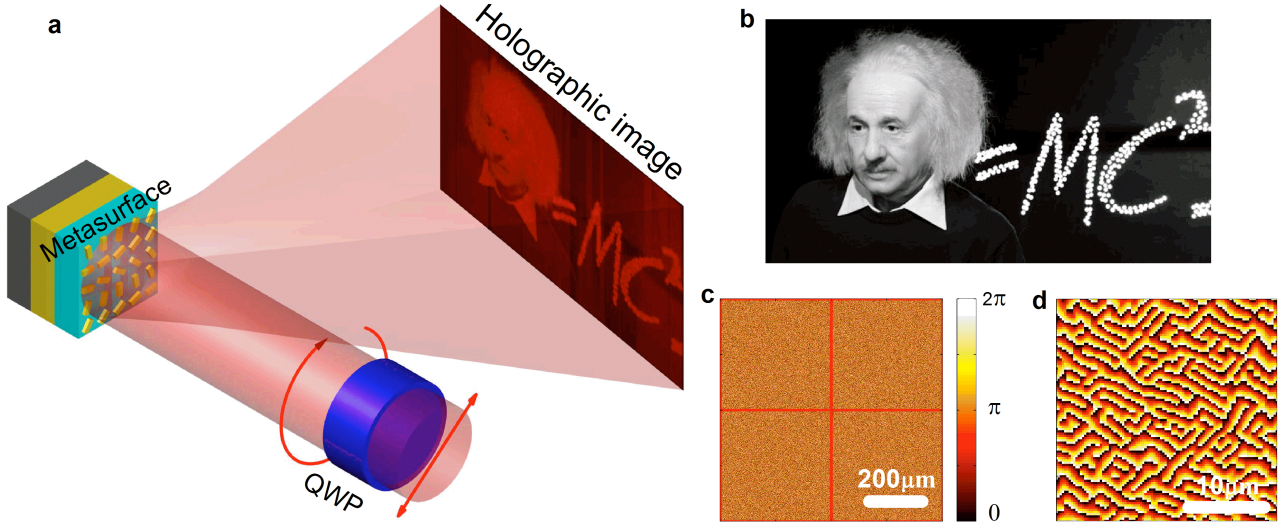

Figure 2 | Working principle and phase distribution of the periodic hologram. a, Illustration of the reflective nanorod-based CGH under a circularly polarized incident beam. The circularly polarized incident beam, which is converted from a linear polarized one by passing through a quarter waveplate (QWP), falls on the metasurface. The reflected beam forms the holographic image in the far-field (at any plane vertical to the optical axis of incident beam). **b**, Target image with 256 greyscale levels and a size of 550×300 pixels used for the generation of the hologram. **c**, To generate the target holographic image in the far field, the designed 16-level phase distribution with 2×2 periods and a scale bar of 200 μm is illustrated. **d,** An enlarged phase distribution with 100×100 pixels and a scale bar of 10 μm at up-left corner of **c** is shown separately.

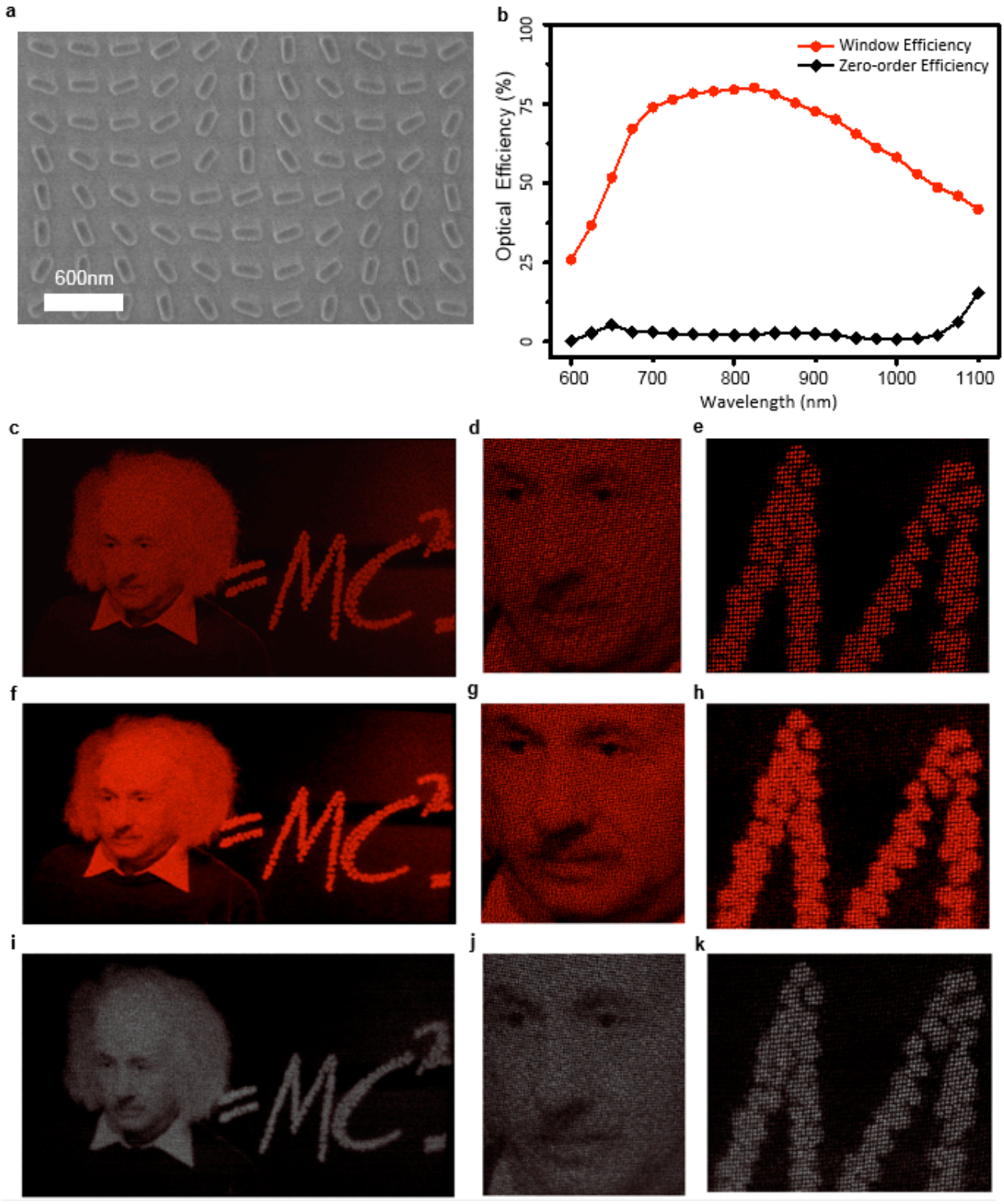

Figure 3 | Experimental results for the holographic image generation. **a**, Scanning electron microscopy image of the fabricated nanorod array (partial view). **b**, Experimentally obtained optical efficiency for both image and 0^{th}-order beam. The measurements show very high optical efficiency above 50% for the image beam over a range of 630-1050 nm. **c, d and e**, Simulated holographic image of Einstein's portrait with enlarged zoom of his face and the character '*M*'. **f, g and h**, Experimentally obtained images that are captured by a visible camera in a far field. The operation wavelength is 632.8 nm. **i, j and k**, Experimentally obtained images that are captured by an infrared camera in the far field,

the operation wavelength is 780 nm.